Tuning the metal-insulator transition in d^1 and d^2 perovskites by epitaxial strain: A first-principles-based study

Gabriele Sclauzero, Krzysztof Dymkowski, and Claude Ederer*
Materials Theory, ETH Zürich, Wolfgang-Pauli-Strasse 27, 8093 Zürich, Switzerland
(Received 12 August 2016; revised manuscript received 21 October 2016; published 5 December 2016)

We investigate the effect of epitaxial strain on the Mott metal-insulator transition (MIT) in perovskite systems with d^1 and d^2 electron configurations of the transition metal (TM) cation. We first discuss the general trends expected from the changes in the crystal-field splitting and in the hopping parameters that are induced by epitaxial strain. We argue that the strain-induced crystal-field splitting generally favors the Mott-insulating state, whereas the strain-induced changes in the hopping parameters favor the metallic state under compressive strain and the insulating state under tensile strain. Thus the two effects can effectively cancel each other under compressive strain, while they usually cooperate under tensile strain, in this case favoring the insulating state. We then validate these general considerations by performing electronic structure calculations for several d^1 and d^2 perovskites, using a combination of density functional theory (DFT) and dynamical mean-field theory (DMFT). We isolate the individual effects of strain-induced changes in either hopping or crystal-field by performing DMFT calculations where we fix one type of parameter to the corresponding unstrained DFT values. These calculations confirm our general considerations for $SrVO_3$ (d^1) and $LaVO_3$ (d^2), whereas the case of $LaTiO_3$ (d^1) is distinctly different, due to the strong effect of the octahedral tilt distortion in the underlying perovskite crystal structure. Our results demonstrate the possibility to tune the electronic properties of correlated TM oxides by using epitaxial strain, which allows to control the strength of electronic correlations and the vicinity to the Mott MIT.

DOI: 10.1103/PhysRevB.94.245109

I. INTRODUCTION

Using modern growth techniques, it is nowadays possible to create high-quality epitaxial thin films and heterostructures of complex transition metal (TM) oxides with well-defined composition and atomically sharp interfaces. Thereby, epitaxial strain, which is caused by the lattice mismatch between thin film and substrate materials, has emerged as a very effective tool to design and optimize specific functional properties [1–3]. For example, epitaxial strain has been shown to strongly affect ferroelectric Curie temperatures and polarization [4–6], and even induce ferroelectricity in otherwise nonferroelectric materials [7,8]. In magnetic materials, epitaxial strain can be used to tune magnetic anisotropy and switch between in-plane and out-of-plane anisotropy [9,10]. Furthermore, strain also affects ionic transport and catalytic properties [11] and allows to tune electronic band gaps [12,13] or Fermi surfaces [14,15].

Particularly interesting are also systems where epitaxial strain can induce a metal-insulator transition (MIT) [16]. Examples of systems where strain-induced MITs have been reported include nickelates [17,18], iridates [19], and titanates [20–22]. Incorporation of such materials in thin films and heterostructures allows to tune the characteristics of the MIT and offers the perspective for novel electronic devices based on the resulting orders-of-magnitude changes in electrical, thermal, and optical properties [23,24].

We have recently shown, using first-principles electronic structure calculations combined with dynamical mean-field theory (DMFT) [25,26], that $LaTiO_3$, which in its unstrained bulk form is a Mott insulator [16,27,28], becomes metallic under a compressive strain of around -2% [21]. On the other hand, similar calculations indicate that the Mott-insulating character of the closely-related material $LaVO_3$ is much less affected by strain, and that $LaVO_3$ remains insulating under both compressive and tensile strain [29].

These computational results are in good agreement with experimental studies that observe metallic, bulklike, conductivity in compressively strained thin films of $LaTiO_3$ grown on $SrTiO_3$ [20,30]. Similar experiments for thin films of $LaVO_3$ grown on $SrTiO_3$ also observe metallic conductivity, however, in this case the conductivity seems to be restricted to the interface region between the thin film and the substrate, which indicates that the metallic character of $LaVO_3$ thin films is not due to epitaxial strain [20].

It is important to note that many different factors can play a role in determining the properties of oxide thin films and heterostructures. In particular, metallic behavior of otherwise insulating materials can be caused by several different effects. Apart from epitaxial strain, important factors are structural and electronic reconstruction at the interface [31,32], the specific interface chemistry [32,33], confinement effects [34,35], or defects [36–38]. The interplay between these effects as well as their relative importance is generally not known *a priori*. However, our previous work on $LaTiO_3$ has clearly shown that epitaxial strain can be a major factor that needs to be taken into account to correctly interpret experimental observations.

In view of this, and considering the different strain responses of closely related materials such as $LaTiO_3$ and $LaVO_3$, it is desirable to build up a comprehensive understanding of how epitaxial strain affects the electronic properties in early TM perovskites, and in particular their tendency to form a Mott-insulating state. To this end, here, we examine the effect of epitaxial strain on the MIT in perovskite TM oxides with d^1 and d^2 electron configurations on the TM cation, such as $LaTiO_3$, $SrVO_3$, and $LaVO_3$. As outlined below, we describe

*claude.ederer@mat.ethz.ch

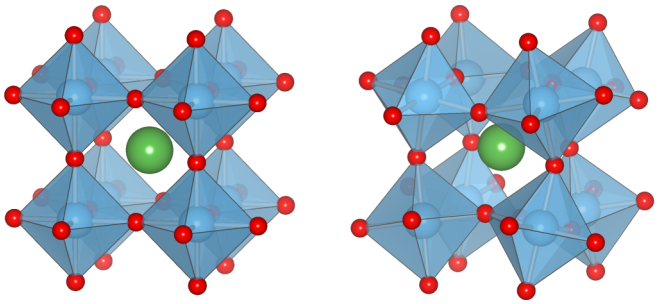

FIG. 1. (Left) Ideal cubic perovskite structure. The TM cations (blue) form a simple cubic lattice and are octahedrally coordinated by anions (red). The larger A-site cations (green) occupy the voids formed in between eight anion octahedra. (Right) Distorted perovskite structure exhibiting tilted octahedra. The depicted case corresponds to $Pbnm$ space group symmetry.

all these systems using an effective three-orbital model with different integer occupations. This type of model has been shown to give a good description of the low-energy electronic properties of early transition metal perovskite oxides [39,40] and is also well suited for a systematic study.

Within the perovskite crystal structure, the TM cation is octahedrally coordinated by oxygen ligands (see Fig. 1). Thus the d-orbital manifold of the TM cation is split by the octahedral component of the crystal field into three t_{2g} and two e_g orbitals.[1] Hybridization of the TM t_{2g} orbitals with the p orbitals of the surrounding oxygen ligands leads to the formation of a partially filled group of bands, in the following denoted "t_{2g} bands", which governs the low energy electronic properties of the early TM perovskites with one or two d electrons on the TM cation [39,40].

In the following, in Sec. II, we first discuss some simple ideas on how strain is expected to affect the electronic structure of these t_{2g} bands, and what general trends can be expected from this. After this general discussion, we present a detailed study of the effect of strain in the prototypical system $SrVO_3$ (Sec. IV A), which in the bulk exhibits a perfect cubic perovskite structure without octahedral rotations (see Fig. 1). We analyze the effect of strain on the t_{2g} bands of $SrVO_3$ in terms of crystal-field splittings and hopping amplitudes. These quantities are obtained by constructing maximally localized Wannier functions corresponding to the t_{2g} bands, obtained for the strained structures within Kohn-Sham density functional theory (DFT). Then, we perform DMFT calculations based on these electronic bands and monitor the effect of strain on the critical interaction strength for the Mott MIT.

In order to clearly distinguish the effect of the strain-induced crystal-field splittings between the t_{2g} orbitals from the effect of the strain-induced changes in the hopping amplitudes, and to make a better connection to our previous results for $LaTiO_3$ and $LaVO_3$, in Sec. IV, we present additional DMFT calculations for all three materials, where we fix either the hopping amplitudes or the crystal-field splitting to the corresponding unstrained values and only consider the strain-induced changes in the respective other quantity.

[1]In most cases, the actual site symmetry is lower than cubic, due to the presence of small structural distortions, in particular rotations of the oxygen octahedra around the central TM cation. In spite of such symmetry lowering, in the following, we are using the labels "t_{2g}" and "e_g" to denote subsets of d orbitals.

TABLE I. Summary of the different effects of compressive (comp.) and tensile (tens.) strain for the three different materials studied in this work. The individual effects of the strain-induced changes in the hopping amplitudes (t_{nm}^{IJ}) and crystal-field parameters (ε_{nm}^{IJ}) are shown in the first and second rows, respectively. The third row ("total") gives the overall net effect. "I" ("M") indicates a tendency to become more insulating (metallic).

	$SrVO_3$ (d^1)		$LaTiO_3$ (d^1)		$LaVO_3$ (d^2)	
	comp.	tens.	comp.	tens.	comp.	tens.
t_{nm}^{IJ}	M	I	M	I	M	I
ε_{nm}^{I}	I	I	M	I	I	I
total	–	I	M	I	–	I

The trends found for all three materials under both compressive and tensile strain are summarized in Table I. Based on these results, which will be described in detail in the remainder of this paper, the following conclusions can be drawn. (1) In all cases, the strain-induced changes in the hopping parameters favor the metallic state under compressive strain and the Mott-insulating state under tensile strain. (2) In $SrVO_3$ and $LaVO_3$, the strain-induced changes in the crystal-field parameters favor the insulating state for both types of strain. As we will discuss in the following, this is the generally expected trend. $LaTiO_3$ behaves differently, due to the strong effect of the octahedral tilts in this material. (3) In total, we find that in all cases tensile strain favors the Mott insulating state. (4) Under compressive strain, the effects stemming from the crystal-field parameters and hopping amplitudes effectively cancel each other in $SrVO_3$ and $LaVO_3$, leaving the critical interaction strength for the Mott transition nearly unchanged compared to the unstrained case. This is the expected "normal" behavior, whereas $LaTiO_3$ becomes metallic under compressive strain, due to the different effect of the crystal-field parameters in this material.

These trends, observed for three representative materials, can easily be applied also to other perovskites with d^1 and d^2 electron configuration of the TM cation. Our work thus allows to make predictions about the effect of epitaxial strain on the electronic properties of other d^1 and d^2 perovskite systems, and thus provides useful guidance for future studies of these materials in thin films and as components of oxide heterostructures.

II. GENERAL CONSIDERATIONS ON THE EFFECT OF EPITAXIAL STRAIN

If a material is epitaxially grown on a substrate without forming dislocations, then the extensions of the crystallographic unit cell in the plane parallel to the substrate surface are constrained to the corresponding lattice constants of the substrate, whereas the unit cell can freely adjust in the perpendicular direction. This elastic deformation of the unit cell will affect bond distances and, potentially, bond angles even far away from the substrate-film interface.

In this section, we discuss the expected effect of these structural changes on the electronic properties of early transition metal perovskites, using a tight-binding (TB) description for the partially-filled t_{2g} bands formulated in a basis of "effective" t_{2g} orbitals centered on the TM cations. Such a TB description can be obtained, e.g., by constructing maximally localized Wannier functions from the corresponding Kohn-Sham bands [41,42]. The resulting t_{2g}-like Wannier functions are typically more extended than atomic orbitals and also contain contributions on the surrounding oxygen sites stemming from hybridization between atomic-like cation d orbitals with oxygen p orbitals (see, e.g., Refs. [21,40,42]).

The general form of such a TB Hamiltonian is as follows:

$$H_0 = \sum_{I,m,n} \varepsilon^I_{nm} d^\dagger_{In} d_{Im} + \sum_{I,J,m,n} t^{IJ}_{nm} (d^\dagger_{In} d_{Jm} + d^\dagger_{Jm} d_{In}). \quad (1)$$

Here, I and J indicate different TM sites, m and n indicate different orbitals centered at these sites, and $d^\dagger_{In}$ is the creation operator for an electron on site I in orbital n. Since there is no explicit spin dependence in Eq. (1), the spin index has been suppressed for more clarity.

The first term in Eq. (1) contains the on-site *crystal-field energies* ε^I_{nm}, which can be obtained as matrix elements of the Hamiltonian between Wannier orbitals centered on the same site I. The second term in Eq. (1) contains the inter-site *hopping amplitudes* t^{IJ}_{nm}, which are obtained as matrix elements of the Hamiltonian between Wannier orbitals centered on different sites I and J. In general, the strain-induced changes in bond lengths and bond angles affect both the crystal-field energies and the hopping parameters.

In order to describe a Mott insulator (or a metallic system close to a Mott-insulating state), the noninteracting Hamiltonian in Eq. (1) has to be supplemented by a term representing the on-site electron-electron interaction. We use the so-called Slater-Kanamori form (see, e.g., Ref. [43]):

$$\begin{aligned} H_{\text{int}} = & \sum_n U n_{n,\uparrow} n_{n,\downarrow} + \sum_{n \neq m,\sigma} U' n_{n,\sigma} n_{m,-\sigma} \\ & + \sum_{n \neq m,\sigma} (U' - J) n_{n,\sigma} n_{m,\sigma} \\ & - \sum_{n \neq m} J (d^\dagger_{n,\downarrow} d^\dagger_{m,\uparrow} d_{m,\downarrow} d_{n,\uparrow} + d^\dagger_{m,\uparrow} d^\dagger_{m,\downarrow} d_{n,\uparrow} d_{n,\downarrow} + \text{H.c.}). \end{aligned} \quad (2)$$

Here, $d^\dagger_{n,\sigma}$ is the creation operator for an electron in orbital n with spin σ, and $n_{n,\sigma} = d^\dagger_{n,\sigma} d_{n,\sigma}$. The parameters U, U', and J describe the strength of the intra- and interorbital electron-electron interaction and the Hund's rule coupling, respectively, and $U' = U - 2J$. The site index I has been suppressed in Eq. (2), since all terms are purely local.

A. Crystal-field splitting

We first discuss the effect of the strain-induced crystal-field splitting between the effective t_{2g} Wannier orbitals. We consider the case of an ideal perovskite structure without octahedral rotations [see Fig. 1(a)], and we assume that the surface of a hypothetical substrate can be represented by a two-dimensional square lattice oriented parallel to the (001) plane (x-y plane) of the perovskite. We further assume that the thin film adopts the in-plane lattice constant of the underlying substrate whereas the out-of-plane lattice constant adjusts to minimize the elastic energy of the system. In general, this will lead to a tetragonal deformation of the perovskite unit cell.

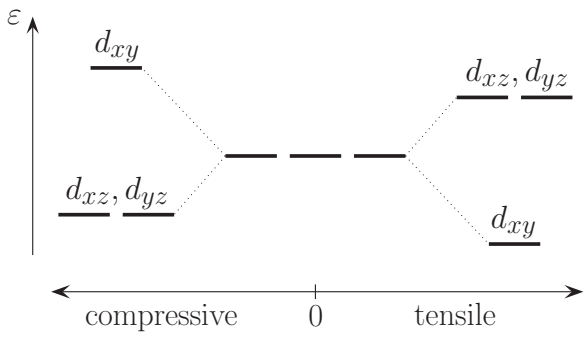

FIG. 2. Schematic depiction of the crystal-field splitting between t_{2g} orbitals induced under compressive and tensile epitaxial strain, respectively. Here, the x-y plane is oriented parallel to the surface of the hypothetical substrate.

The resulting crystal-field energies in Eq. (1) are diagonal and do not depend on the site index I, i.e. $\varepsilon^I_{nm} = \varepsilon_m \delta_{nm}$. The crystal-field associated to the epitaxial strain reduces the symmetry of the perovskite crystal structure from cubic to tetragonal, lifting the threefold degeneracy among the t_{2g} orbitals into a doubly degenerate (d_{xz} and d_{yz}) and a nondegenerate (d_{xy}) set of orbitals, as shown schematically in Fig. 2. Under compressive strain, the oxygen ligands within the x-y plane move closer to the central TM cation. This strongly increases the hybridization of the d_{xy} orbital with its surrounding ligand O-p states, thus shifting the d_{xy} orbital to higher energies relative to the d_{xz}/d_{yz} orbitals due to the antibonding character of the t_{2g} states. Analogously, under tensile strain, the increase of the TM-O bond distances within the x-y plane lowers the energy of the d_{xy} orbital relative to d_{xz}/d_{yz}.

The effect of such a crystal-field splitting on the Mott MIT in a simple three-band Hubbard model, applicable to systems with partially filled t_{2g} states, has been studied in Ref. [43] (see also Refs. [44,45]). It was found that for both one- and two-electron-filling, i.e., corresponding to a d^1 and d^2 electron configuration of the TM cation, the crystal-field splitting reduces the critical value for the Hubbard U parameter that is required to obtain an insulating state. A similar result has also been reported for the two-band Hubbard model including a crystal-field splitting [46]. This can be understood from the fact that the splitting reduces the orbital degeneracy, and, as shown in Refs. [47,48], the critical U decreases with decreasing orbital degeneracy. A particularly strong reduction of the critical U was found for the case with two orbitals at lower energy and one orbital at higher energy, i.e., corresponding to compressive strain, and two electrons per site [43]. In this case, the two lower-lying orbitals are effectively half-filled, and the Hund's rule interaction between the two electrons, represented by the parameter J in (2), leads to a strong stabilization of the Mott insulating state. Thus a strain-induced crystal-field

splitting is generally expected to favor the insulating state, with a particularly strong effect for a d^2 system under compressive strain.

B. Hopping amplitudes

While the effect of a crystal field on the Mott transition has already been studied within a simplified three orbital Hubbard model [43–45], we are not aware of any systematic studies on how the strain-induced modifications of the hopping parameters, t_{nm}^{IJ} in Eq. (1), will affect the MIT. In the following, we therefore discuss how the hopping parameters are affected by epitaxial strain, and what resulting effects on the electronic properties can be expected.

We first note that the hopping between two effective t_{2g} Wannier functions located at adjacent TM sites should be viewed as an *effective* hopping process that is mediated by the oxygen anion situated between the two TM cations, i.e., an electron first hops from one of the TM sites into a p orbital on the oxygen site and then onto the other TM site. Thus the effective t_{2g}-t_{2g} hopping amplitude is determined mostly by the TM-O bond length and by the TM-O-TM bond angle, whereas the direct TM-TM distance is less important.

Compressive epitaxial strain reduces the TM-O bond distances in the two in-plane directions, i.e., parallel to the film-substrate interface, and increases the bond distance in the perpendicular direction, due to the outward relaxation of the out-of-plane lattice parameter. This leads to increased in-plane hopping amplitudes and reduced out-of-plane hoppings compared to the unstrained case. Tensile epitaxial strain has the opposite effect.

On the other hand, if octahedral rotations are present in the structure (see Fig. 1), as is the case for most perovskites, then the TM-O-TM bond angles are distorted from the ideal value of 180° and the amount of this distortion will change with strain. In general, the in-plane bond angles will become more distorted under compressive strain, whereas the out-of plane bonds will be straightened out,[2] i.e., the corresponding bond angles will become less distorted (see, e.g., Refs. [21,29,49]). Since the hopping amplitudes decrease with increasing distortion of the bond angles, i.e., with increasing deviation from the ideal value of 180°, this leads to decreasing in-plane hopping amplitudes and increasing out-of-plane hoppings under compressive strain. Again, tensile strain leads to the opposite trends.

Thus it can be seen that the trends expected from the strain-induced changes in the TM-O-TM bond angles are exactly opposite to those expected from the strain-induced changes in the bond distances. Our previous calculations for $LaTiO_3$ and $LaVO_3$ indicate that in both materials the influence of the bond distances dominates, i.e., the in-plane hoppings are increased under compressive strain and the out-of-plane hoppings are decreased (and vice versa for tensile epitaxial strain) [21,29].

[2]We note that in the presence of octahedral rotations, the TM-O bonds are not exactly parallel or perpendicular to the substrate plane. Nevertheless, for typical octahedral rotation angles smaller than 15°–20°, a clear distinction between in-plane and out-of-plane oriented bonds is easily possible.

How will these changes of the hopping amplitudes affect the Mott MIT? For the simplest case with one orbital per site, the Mott transition is governed by the ratio U/W, where W is the corresponding bandwidth [25]. The present case with three orbitals is more complex. However, to a good approximation, the t_{2g} bands can be viewed as three independent bands corresponding to d_{xy}, d_{xz}, and d_{yz} orbitals, respectively. From the above considerations it therefore follows that the bandwidth of the d_{xy}-derived band, which is determined by the in-plane hopping, will increase under compressive strain and decrease under tensile strain. On the other hand, the d_{xz}-derived bands—as well as the d_{yz}-derived—will become more anisotropic but, to a first approximation, the total width of these bands will only be weakly affected by epitaxial strain, since the increase of the in-plane hopping under compressive strain will, at least partially, be compensated by the decrease in the out-of-plane hopping. Overall, these strain-induced modifications of the nearest-neighbor hopping amplitudes lead to a moderate increase of the total t_{2g} bandwidth under compressive strain and to a slight decrease of bandwidth under tensile strain, as also confirmed by our previous DFT calculations for $LaTiO_3$ and $LaVO_3$ [21,29].

Thus one can expect that the increase in bandwidth under compressive strain will favor the metallic state, whereas the reduced bandwidth under tensile strain will be more favorable for the Mott-insulating state. However, it is not clear *a priori* how the strain-induced anisotropy in the d_{xz}- and d_{yz}-derived bands will affect the MIT. Systematic model calculations are required to explore this issue. Furthermore, the difference in bandwidth for the d_{xy}-derived band compared to the other two bands could potentially lead to orbitally-selective Mott transitions [50,51]. Another effect, which, however, is not straightforward to incorporate systematically into a simplified TB model, is that the presence of octahedral tilts leads to mixing between the three bands corresponding to the three different orbital characters. Again, it is unclear how such intermixing will affect the MIT.

In this work, we are not aiming for a full clarification of all these issues. Instead, we verify the simple general considerations outlined in this section using realistic first-principles-based electronic structure calculations for different d^1 and d^2 perovskite TM oxides under epitaxial strain. Before presenting our results, we briefly summarize the (expected) net effect of the strain-induced changes in crystal-field splitting and hopping amplitudes on the MIT.

C. Expected strain dependence of the MIT

As outlined in the preceeding sections, the strain-induced crystal-feld splitting will always lower the critical U for the Mott transition and promote the insulating phase. On the other hand, we expect the strain-related changes in the hopping amplitudes to increase the critical U under compressive strain and decrease it under tensile strain. Thus partial cancellation between the crystal-field- and hopping-related effects can occur under compressive strain, whereas tensile strain is expected to promote insulating behavior in all cases.

The opposing trends resulting from crystal-field splitting and hopping amplitudes under compressive strain, have already been suggested as explanation for the weak effect of

compressive strain on the MIT in the d^2 system $LaVO_3$ [29]. On the other hand, it has been found that tensile strain strongly reinforces the insulating character of the d^1 Mott insulator $LaTiO_3$ [21], and also increases the critical U in the d^2 system $LaVO_3$ [29]. Furthermore, the discussed trends also indicate that a metallic d^1 or d^2 system, such as, e.g., $SrVO_3$, is expected to move closer to the Mott-insulating state, and might even become insulating under strong tensile strain.

We note that in our discussion we have assumed that the interaction parameters, U and J, are not affected by the epitaxial strain. Thus we assume that the screening of the electron-electron interaction is not significantly affected by the strain-induced structural modifications. Even though this might indeed be a good approximation, the corresponding quantitative changes remain to be verified.[3]

III. COMPUTATIONAL METHOD

To validate the general considerations outlined in the previous section, we perform electronic structure calculations for a set of representative materials using density functional theory (DFT) [52,53] in combination with dynamical mean-field theory (DMFT) [25].

We address the effect of epitaxial strain, by using bulk unit cells with periodic boundary conditions in all three dimensions, where we constrain the lattice parameters in the two directions corresponding to the substrate plane, while relaxing all other structural degrees of freedom. Thus we do not explicitly consider a substrate in our calculations, e.g., by using a slab geometry and large supercells. Consequently, our approach allows to clearly distinguish the bulk-like strain effect from other factors related to the interface between the thin film material and the substrate.

Most systems investigated in this work exhibit a distorted perovskite structure with space group symmetry $Pbnm$ in their bulk forms. We consider the case where the substrate presents a square lattice on its surface, and we assume a growth geometry where the two shorter lattice vectors of the orthorhombic $Pbnm$ structure are parallel to the surface plane of the substrate and are constrained to have equal length. The longest lattice vector of the $Pbnm$ structure is then oriented perpendicular to the substrate plane and is allowed to adjust its length in order to minimize the energy of the system under the epitaxial constraint. Simultaneously, all internal structural degrees of freedom related to the individual atomic positions are also relaxed. The chosen geometry preserves the $Pbnm$ symmetry of the bulk system and allows for a systematic comparison between the different materials considered in this work. The case of $SrVO_3$, which in its bulk form exhibits a perfect cubic perovskite structure with $Pm\bar{3}m$ space group symmetry, is treated analogously, i.e., assuming growth along the [001] direction on a square lattice substrate.

The applied strain is defined as $s = (a - a_0)/a_0$, where a is the constrained in-plane lattice constant (corresponding to the surface lattice constant of the hypothetical substrate) and a_0 is the unstrained reference lattice constant of the thin film material. For $SrVO_3$, a_0 is the theoretical equilibrium lattice constant of the ideal perovskite ($Pm\bar{3}m$) structure, while for the orthorhombic $Pbnm$ systems $LaTiO_3$ and $LaVO_3$, a_0 was taken as the in-plane lattice parameter that minimizes the total-energy under the epitaxial constraint (i.e., with $a = b$) [21].

DFT calculations within the generalized gradient approximation according to Perdew, Burke, and Ernzerhof (PBE) [54] allow us to relax the crystal structure under the epitaxial constraint and to obtain the corresponding electronic band structure. We employ the QUANTUM ESPRESSO (QE) package [55] with ultrasoft pseudopotentials [56] from the QE website. Semicore states of the different cations are included in the valence ($3s$ and $3p$ for V and Ti, $4s$ and $4p$ for Sr, $5s$ and $5p$ for La), while projectors for the empty La-$4f$ shell are not included in the potential. The plane-wave cutoffs used to represent the wave functions (charge density) are 60 Ry (500 Ry) for $SrVO_3$, 40 Ry (480 Ry) for $LaTiO_3$, and 40 Ry (300 Ry) for $LaVO_3$. The Brillouin zone was sampled with a regular k-point grid with dimensions $6 \times 6 \times 4$ for $LaTiO_3$ and $LaVO_3$ and $8 \times 8 \times 8$ for $SrVO_3$.

We note that since we are interested in the paramagnetic structures at room temperature, we are performing non-spin-polarized calculations. In general, we obtain good agreement with the known bulk structures for all materials studied in this work (see also Refs. [21,29]). We note that these crystal structures do not exhibit any distortions that are specifically driven by the electron-electron interaction (e.g., Jahn-Teller distortions) and thus a PBE treatment is sufficient to obtain accurate structural properties.

After relaxing the structure under the epitaxial constraint, corresponding to different in-plane lattice constants, we construct a representation of the electronic bands with predominant TM-t_{2g} orbital character using maximally localized Wannier functions (MLWFs) [41,57]. The MLWFs are constructed from initial projections on d_{xy}, d_{xz}, and d_{yz}-type orbitals, and we always use a coordinate system where the cartesian axis are approximately oriented along the direction of the TM-O bonds, with the z axis perpendicular to the surface of the hypothetical substrate.

The Kohn-Sham Hamiltonian for the t_{2g} bands, expressed in the basis of MLWFs, has precisely the form of Eq. (1), and is used as noninteracting part of a multi-band Hubbard Hamiltonian, where the Slater-Kanamori form, Eq. (2), is used to describe the Coulomb interaction between electrons on the same site. We then perform DMFT calculations for this Hamiltonian [25]. Thus we perform so-called "one-shot" DFT+DMFT calculations, i.e., we do not include full charge self-consistency between the DFT and DMFT parts of the calculation. Previously, it was reported that for the early TM perovskites studied here, full-charge self-consistency leads only to small differences compared to the much faster one-shot calculation [58].

The effective impurity problem obtained within DMFT is solved using a continuous time hybridization expansion quantum Monte Carlo solver [59] implemented within the TRIQS library [60–62]. All DMFT calculations are performed for an inverse temperature of $\beta = 1/(k_B T) = 40\ \mathrm{eV}^{-1}$, corresponding to approximately room temperature. The parameter

[3]We note that the quadratic spread of our Wannier functions for, e.g., $SrVO_3$, changes by less that 1.5% for ±4% strain, which indeed seems a rather small change that is not likely to lead to significant differences in the corresponding U values.

U in Eq. (2) is varied in order to identify the critical value for the MIT for each strain, whereas J is fixed to 0.65 eV, which is a typical value for the materials studied here [21,29,39,40]. Orbital off-diagonal elements of the impurity self-energy are included in the calculations. For more details, we refer to the supplemental material of Ref. [21], where an analogous setup has been used. From the DMFT calculations we obtain the local imaginary time Green's function $G(\tau) = -\langle \hat{T}_\tau d(\tau) d^\dagger(0)\rangle$, where $\hat{T}_\tau$ is the imaginary time-ordering operator. The corresponding spectral function $A(\omega)$ is then constructed using the maximum entropy method [63].

IV. RESULTS AND DISCUSSION

A. $SrVO_3$

We start by discussing the case of $SrVO_3$, where the V^{4+} cation exhibits a formal d^1 electron configuration. $SrVO_3$ is a rare example of a material that exhibits an ideal cubic perovskite crystal structure, i.e., without any symmetry-lowering distortions. $SrVO_3$ is often regarded as a prototypical example for a "correlated metal", i.e., a metallic system where the electron-electron repulsion leads to pronounced mass enhancement and narrowing of the quasiparticle bands. Due to its simple crystal structure and the fact that the t_{2g} bands are well isolated from other bands at higher and lower energies it is often used to test new DFT+DMFT implementations and their extensions [42,64].

The total and projected densities of states (DOS) close to the Fermi energy, ε_F, for unstrained cubic $SrVO_3$, together with its k-resolved band structure, are shown in Fig. 3. It can be seen that there are indeed three partially filled bands with strong atomic V-t_{2g} character that are clearly separated from bands at lower (higher) energies with dominant O-p (V-e_g) character.

We now relax the out-of-plane lattice constant of $SrVO_3$ for fixed in-plane lattice parameters, which are varied by $\pm 4\%$ around the obtained cubic equilibrium lattice constant

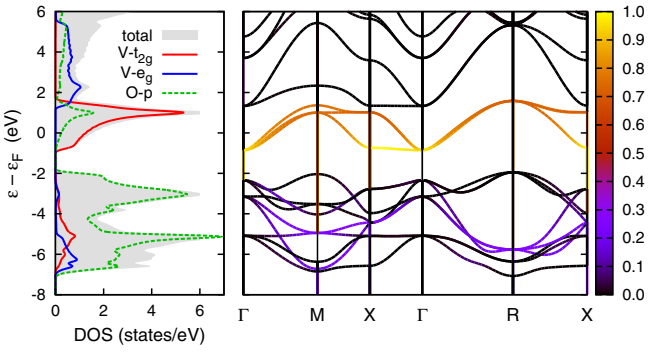

FIG. 3. Electronic structure of unstrained $SrVO_3$ around the Fermi level, ε_F, obtained from DFT. (Left) Total DOS (gray filled area) and partial DOSs (lines) projected onto atomic orbitals with V-t_{2g} (solid red), V-e_g (solid blue), and O-p character (dashed green). (Right) Kohn-Sham eigenvalues along high-symmetry lines in k space. The color represents the amount of V-t_{2g} character within each bands (color scale on the right), with a value of 1 (0) corresponding to maximal (zero) overlap of the corresponding Bloch wave function with the V-t_{2g} atomic orbitals.

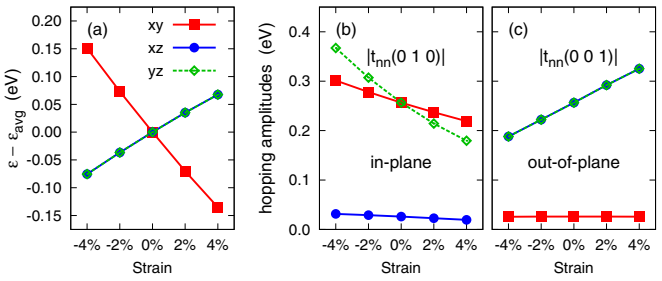

FIG. 4. Crystal-field splitting (a) and nearest-neighbor hopping amplitudes along one of the two equivalent in-plane directions (b) and along the out-of-plane direction (c) in $SrVO_3$ as a function of epitaxial strain. The crystal-field levels in (a) are shown relative to the average t_{2g} orbital energy for each strain.

($a_0 = 3.855$ Å). Due to the high symmetry of $SrVO_3$, with no octahedral rotations, there are no free internal structural parameters. For each strained structure, we then construct MLWFs corresponding to the three V-t_{2g} bands, starting from initial projections on atomic t_{2g} orbitals centered at the V sites. The resulting Wannier orbitals closely resemble the ones of Ref. [42], with strong t_{2g} character on the central V atom and p-like "tails" located on the surrounding oxygen ligands.

Figure 4 shows the strain-dependent crystal-field splitting and nearest neighbor hopping amplitudes, obtained as on-site and intersite matrix elements, respectively, of the Kohn-Sham Hamiltonians of the differently strained structures expressed in the MLWF basis. It can be seen that the crystal-field splitting indeed follows the schematic picture sketched in Fig. 2, with a splitting between d_{xz}/d_{yz} and d_{xy} orbitals that is approximately linear in the strain. The calculated hopping parameters also follow the trends discussed in Sec. II, with the in-plane (out-of-plane) hopping amplitudes decreasing (increasing) with strain. The strain dependence of the in-plane d_{xy} hopping is weaker than that of the d_{xz}/d_{yz} orbitals. The out-of-plane hopping for the d_{xy} orbital and the in-plane hopping along y for the d_{xz} orbital (and along x for the d_{yz} orbital) are very small, as expected from the planar orientation of the t_{2g} orbitals. Note that all interorbital nearest-neighbor hoppings are zero by symmetry.

Next, we perform DMFT calculations for the t_{2g} bands using the Hamiltonian expressed in MLWFs, where we add the electron-electron interaction in the Slater-Kanamori form, Eq. (2). For each strained structure, we vary the interaction parameter U, and identify the critical U for the Mott MIT by monitoring the value of the imaginary time Green's function $G(\tau)$ at $\tau = \beta/2$. $G(\beta/2)$ is a measure of the spectral density at the "Fermi level" $\omega = 0$ (see, e.g., Ref. [65]):

$$A(\omega = 0) = -\frac{1}{\pi} \lim_{\beta\to\infty} \mathrm{Tr}[\beta G(\beta/2)]. \qquad (3)$$

Figure 5(a) shows the trace of $G(\beta/2)$ as function of U for different values of epitaxial strain. It can be seen that in all cases $G(\beta/2)$ is nonzero for small U (i.e., the system is metallic) and exhibits a transition to $G(\beta/2) \approx 0$, i.e., to an insulating state, at some (strain-dependent) critical value of $U = U_{\mathrm{MIT}}$, which indicates the Mott MIT. For unstrained $SrVO_3$ this transition occurs at $U_{\mathrm{MIT}} \approx 6$ eV and this value is

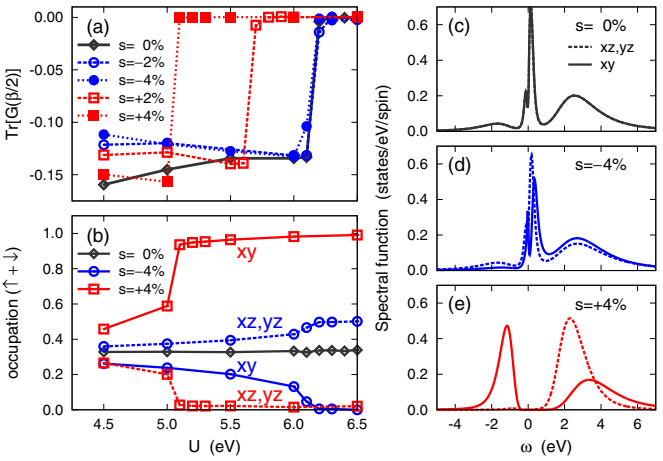

FIG. 5. DMFT results for unstrained $SrVO_3$ (black) and for $SrVO_3$ under tensile (red) or compressive (blue) epitaxial strain. (a) Trace of the Green's function $G(\tau)$ at $\tau = \beta/2$ and (b) orbitally resolved occupations, summed over both spin components, obtained from $-G(\beta)$, as a function of the interaction parameter U. The orbitally resolved spectral function $A(\omega)$ evaluated at $U = 5.5$ eV is plotted as a function of ω for the unstrained case (c), under compressive strain (d), and under tensile strain (e). Different line styles in (b)–(e) differentiate between the d_{xy} orbital (solid) and the degenerate d_{xz}/d_{yz} orbitals (dashed).

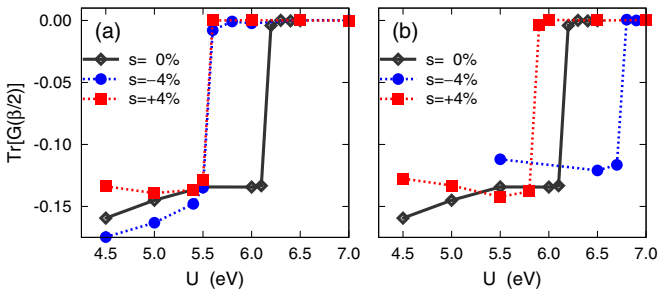

FIG. 6. Separate effects of the strain-induced changes of the crystal-field splitting (a) and of the hopping amplitudes (b), i.e., in (a), the hopping amplitudes are fixed to their unstrained values and in (b) the same is done for the crystal-field splitting. The plots show the evolution of the trace of $G(\beta/2)$ as a function of U under compressive strain (blue) and tensile strain (red) in comparison to the unstrained case (black).

nearly unchanged under compressive strain. In contrast, under tensile strain, there is a clear shift of U_{MIT} to lower values, with $U_{\mathrm{MIT}} \approx 5$ eV for a tensile strain of 4%.

The orbital occupations depicted in Fig. 5(b) show that for zero strain all orbitals are equally populated both in the metallic and in the insulating state (consistent with the cubic symmetry of the system). For the strained systems, the crystal-field splitting leads to an occupation imbalance between the energetically higher- and lower-lying orbitals. While this occupation imbalance is not very pronounced in the metallic state, the higher-lying orbital(s) become completely empty in the insulating state.

It follows from the observed strain-induced shift in U_{MIT}, that for a fixed value of U in the range between 5 eV $\lesssim U \lesssim$ 6 eV, a strain-induced metal-insulator transition occurs at a U-dependent critical strain value $\leqslant$4%. Spectral functions for the case with $U = 5.5$ eV are shown in Figs. 5(c)–5(e). For a tensile strain of 4%, a clear energy gap can be observed. On the other hand, under compressive strain, the quasiparticle peak around $\omega = 0$ eV is slightly broadened compared to the unstrained case, in particular, for the d_{xy} orbital character. This is consistent with the expected trends discussed in Sec. II B.

We note that a value of $U = 5.5$ eV is perhaps slightly too large for $SrVO_3$ [39,40,42], or at least it is at the upper end of the spectrum of U values that are considered suitable to achieve a good description of the electronic properties of this material.[4] It is therefore unclear, whether large enough tensile strains can be achieved in order to observe a strain-induced MIT in thin films of $SrVO_3$. However, we note that, as discussed in Sec. II C below, the strain effect described here can also cooperate with other factors favoring the insulating state in ultra-thin films of $SrVO_3$ (see, e.g. Ref. [66]). Furthermore, we note that it might be worthwhile to test whether the O-p dominated bands starting (within PBE) at approximately 1 eV below the V-t_{2g} bands (see Fig. 3) also affect the strain dependence of the MIT, by including them into the DMFT treatment of strained $SrVO_3$. However, even if it might not be feasible to obtain insulating $SrVO_3$ in epitaxial thin films under tensile strain, our results clearly indicate that tensile epitaxial strain can lead to changes of the quasiparticle effective mass and a partial suppression of orbital fluctuations.

The strong decrease of U_{MIT} under tensile strain is consistent with the general trends expected both from the strain-induced changes in the crystal-field splitting and in the hopping amplitudes, whereas the absence of any shift under compressive strain indicates a possible cancellation between the opposing trends related to crystal-field and hopping. To further verify this picture, and to better isolate the separate effects of the strain-induced changes of the hopping amplitudes from those of the crystal-field splitting, we perform additional calculations where we fix one of the two types of parameters to the corresponding unstrained values and only use the strain-dependent values for the respectively other parameter. The results are depicted in Fig. 6.

From the calculations with fixed "unstrained" hopping parameters [Fig. 6(a)] it can be seen that the strain-induced crystal-field splitting decreases U_{MIT} for both tensile and compressive strain. Interestingly, the shift of U_{MIT} is identical for $\pm$4% strain within the limits of accuracy of our calculations. This is consistent with the previous model calculations of Ref. [43], where the filling dependence of the Mott MIT in

[4]It should also be noted that recent work has shown that the screened Hubbard interaction is in general strongly frequency dependent (see, e.g., Refs. [69,70]). Thus the value of U in the present work should be considered an "effective" parameter that results in the best description of a certain material within this "static U" approximation. This value is not necessarily identical to the value at zero frequency when considering the fully frequency-dependent screened Coulomb interaction.

the three-orbital model has been studied, and the same critical chemical potential for the destruction of the insulating state with one electron per site has been found for both signs of the crystal-field splitting.

On the other hand, Fig. 6(b) reveals that the strain-induced changes in the hopping parameters do affect U_{MIT} in different ways for compressive and tensile strain. The observed trends are the ones expected from the discussion in Sec. II B, i.e., compressive (tensile) strain increases (decreases) U_{MIT} and thus favors the metallic (insulating) phase.

These results confirm that for tensile strain the effects resulting from the strain-induced changes in the crystal-field splitting and hopping parameters cooperate, leading to a pronounced shift of U_{MIT} to lower values, i.e., the system moves closer to the MIT. In contrast, under compressive strain, the effect of the crystal-field splitting counteracts the effect stemming from the changes in the hopping amplitudes, leaving U_{MIT} essentially unaffected. This also shows that for a proper understanding of strain effects on the MIT in correlated materials, the strain-induced changes in both crystal-field and hopping parameters have to be taken into account.

B. $LaTiO_3$ and $LaVO_3$

We now discuss the more complex cases of $LaTiO_3$ and $LaVO_3$. In our previous work, we have already demonstrated that the Mott MIT in the d^1 system $LaTiO_3$ is strongly affected by strain, with tensile strain reinforcing the Mott-insulating character of $LaTiO_3$, and a transition to the metallic state under compressive strain of 1%–2%. [21] Thereby, the crucial difference between the d^1 systems $LaTiO_3$ and $SrVO_3$ is the presence of strong octahedral tilts in $LaTiO_3$, which lower the space group symmetry to orthorhombic $Pbnm$ and distort the TM-O-TM bond angles (see Fig. 1). This distortion of the ideal cubic perovskite structure also leads to a pronounced crystal-field splitting between the t_{2g} orbitals *already* for zero strain and a more complex strain dependence of the hopping parameters compared to $SrVO_3$ [21].

In contrast, for the d^2 system $LaVO_3$, we found that the critical U for the Mott MIT is less affected by epitaxial strain [29]. Tensile strain leads to a moderate decrease of U_{MIT} in $LaVO_3$, i.e., strengthening the insulating state, whereas compressive strain has nearly no effect on U_{MIT} (even though it has a noticeable effect on the orbital polarization among the t_{2g} orbitals). Thus qualitatively the trends in $LaVO_3$ are similar to the case of $SrVO_3$ discussed in the preceding section. The very weak effect of compressive strain on the MIT in $LaVO_3$ has been attributed to opposing effects of the strain-induced changes in crystal-field splitting and bandwidth [29], in analogy to the discussion in Secs. II C and IV A.

In Fig. 7, we compare the calculated crystal-field splitting between the three t_{2g} orbitals of the TM cations in $LaVO_3$ and $LaTiO_3$. The corresponding energies are obtained as eigenvalues of the on-site part of the Kohn Sham Hamiltonian in the basis of MLWFs, i.e., ε_{nm} in Eq. (1). It can be seen that in $LaVO_3$ the strain dependence of the crystal-field splitting follows rather closely the schematic picture shown in Fig. 2, and also observed for $SrVO_3$ in Fig. 4. Thus, in $LaVO_3$, the octahedral tilt distortion results only in a weak splitting between the three t_{2g} orbitals (see also Ref. [67]).

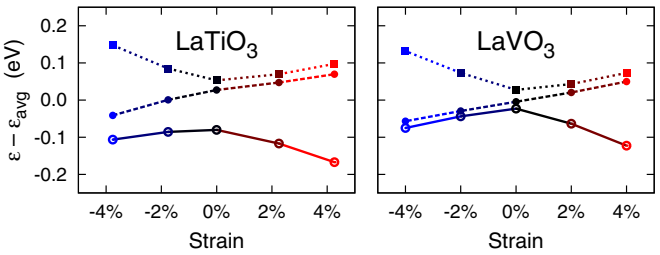

FIG. 7. Strain-dependent crystal-field levels of the three TM t_{2g} orbitals for $LaTiO_3$ (left) and $LaVO_3$ (right). For each strain, the orbital levels are shown with respect to the corresponding average value $\varepsilon_{\mathrm{avg}}$. The data for $LaTiO_3$ is reproduced from Ref. [21].

In contrast, the effect of the octahedral tilts is much stronger in $LaTiO_3$, which exhibits a large crystal-field splitting already in the unstrained state (see left side of Fig. 7) [21,39]. For zero strain, the splitting between the three t_{2g} orbitals resembles the tensile strain case in the schematic picture, with two (nearly degenerate) orbitals at higher energies and one orbital at lower energy. The corresponding splitting is further increased under tensile strain. On the other hand, applying compressive strain reduces the splitting between the lowest and second-lowest orbital and shifts the highest-lying orbital further up in energy. This behavior was already discussed in Ref. [21].

Figure 8 shows the calculated hopping amplitudes for nearest-neighbor (NN) and next-nearest-neighbor (NNN) hopping in $LaVO_3$ as a function of epitaxial strain. It can be seen that the dominant in-plane NN hoppings are decreasing (increasing) under tensile (compressive strain) and vice versa

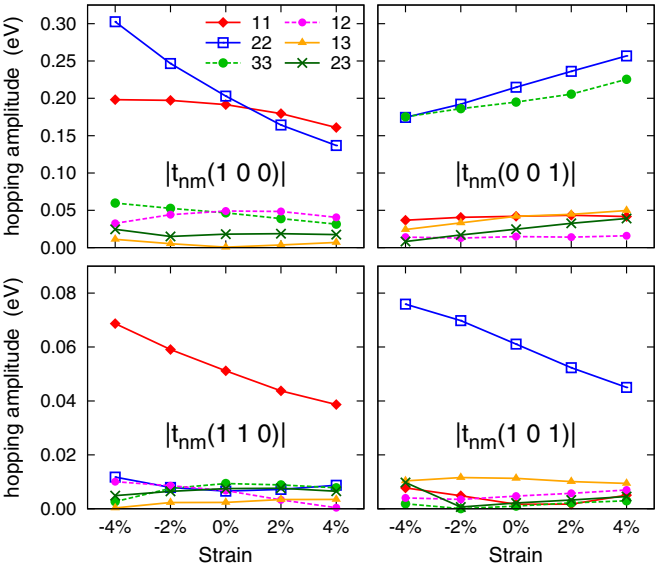

FIG. 8. Strain dependence of nearest-neighbor (NN, top) and next-nearest-neighbor (NNN, bottom) hopping amplitudes in $LaVO_3$. The left panels corresponds to in-plane hoppings (along x for NN and along $x + y$ for NNN), the right panels correspond to out-of-plane hoppings (z for NN and $x + z$ for NNN). Orbital "1" roughly corresponds to d_{xy} and is oriented mostly in-plane, while orbitals "2" and "3" derive from d_{xz} and d_{yz}, respectively (see text).

for the out-of-plane hoppings. This closely resembles the trends observed for $SrVO_3$ in Fig. 4, and demonstrates that the changes in the hopping amplitudes are indeed dominated by the changes in the TM-O bond lengths and not by the changes in the TM-O-TM bond angles (see discussion in Sec. II). The MLWFs in $LaVO_3$ reflect approximately the shape and orientation of the t_{2g} orbitals used to construct their initial projections (d_{xy}, d_{xz}, and d_{yz} for orbitals 1, 2, and 3, respectively), even though this is not enforced by symmetry. Thus the off-diagonal NN hoppings as well as, e.g., the hopping along x for the d_{yz}-derived MLWF remain small. The dominant NNN hopping corresponds to the diagonal directions within the plane in which the corresponding MLWFs are oriented, and are about a factor 4 smaller than the dominant NN hoppings. They exhibit a similar strain dependence as the dominant NN in-plane hoppings.

Thus, as for the crystal-field splitting, the effect of the octahedral tilts on the hopping amplitudes is relatively weak in $LaVO_3$. The main effect is simply an overall reduction of the dominant hopping amplitudes. Calculations for $LaVO_3$ in a hypothetical ideal cubic pervskite structure (not shown here) lead to hopping amplitudes that are about 25% larger than for $Pbnm$ $LaVO_3$, and are comparable to the hopping amplitudes obtained for $SrVO_3$. We also note that such a hypothetical cubic $LaVO_3$ has a critial U for the Mott MIT of about 5.1 eV, i.e., almost 1 eV larger than in $Pbnm$-$LaVO_3$ [29]. Thus cubic $LaVO_3$ would be very close to the MIT or even be metallic. Therefore, it appears that, similar to $LaTiO_3$ [39], the insulating state in $LaVO_3$ is stabilized by the octahedral tilt distortion. However, in contrast to $LaTiO_3$, the crucial effect in $LaVO_3$ is not a suppression of orbital fluctuations due to a strong crystal-field splitting, but rather the resulting reduction of hopping amplitudes.

Next, we present further analysis of the effect of epitaxial strain on the electronic properties of $LaTiO_3$ and $LaVO_3$. In order to clearly distinguish the effects resulting from the strain dependence of the crystal-field splitting and from the strain dependence of the hopping parameters, we perform DMFT calculations for strained $LaTiO_3$ and $LaVO_3$ in the same way as described in Sec. IV A for $SrVO_3$, i.e., we fix either the crystal-field or the hopping parameters to their unstrained values, while using the strain-dependent values for the respectively other type of parameter. The corresponding results, depicting the evolution of Tr $G(\beta/2)$ as function of U for each case, are summarized in Fig. 9.

It can be seen that the effect of the strain-dependent hopping parameters on U_{MIT} (bottom panels in Fig. 9) is similar in both $LaTiO_3$ and $LaVO_3$, and follows the general trends discussed in Sec. II B and also observed for $SrVO_3$ in Fig. 6. Tensile (compressive) strain shifts U_{MIT} to lower (higher) values. These shifts of U_{MIT} are somewhat larger in $LaTiO_3$ than in $LaVO_3$.

In contrast, the effect of the strain-induced crystal-field splitting (top panels in Fig. 9) is qualitatively different in $LaVO_3$ and $LaTiO_3$. In $LaVO_3$, U_{MIT} is reduced under both compressive and tensile strain, as expected from the strain-induced crystal-field splitting (see Sec. II A) and similar to the case of $SrVO_3$ (see Fig. 5). The reduction of U_{MIT} is stronger under compressive strain, which for a d^2 system leads to a situation with effective half-filling. However, for both types of

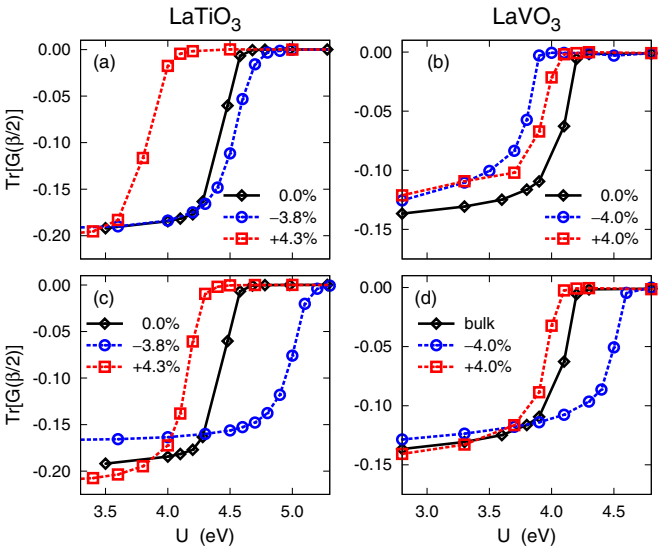

FIG. 9. Separate effects of the strain-dependent crystal-field splitting, i.e., hopping parameters fixed to the unstrained values, (top) and of the strain-dependent hopping parameters, i.e., crystal field fixed to the unstrained values, (bottom) for $LaTiO_3$ (left) and $LaVO_3$ (right).

strain the decrease of U_{MIT} in $LaVO_3$ is significantly weaker than for $SrVO_3$.

The case of $LaTiO_3$ is rather different. The critical U for the MIT is strongly reduced under tensile strain and is slightly increased under compressive strain. This is due to the strong crystal-field splitting already present in the unstrained state. Applying compressive strain reduces the already existing crystal-field splitting between the two energetically lowest orbitals and thus moves the system closer to a situation with one electron in two degenerate orbitals. This disfavors the insulating state and increases U_{MIT} [47,48]. On the other hand tensile strain strongly increases the splitting between the lower-lying d_{xy}-like and the other two t_{2g} orbitals, which has the "normal" effect of lowering U_{MIT}.

Thus, in $LaTiO_3$, the effects of crystal-field splitting and hoppings cooperate for both types of strain. It is interesting to note, though, that the increase of U_{MIT} under compressive strain that is caused by the strain-dependent hopping amplitudes is much larger than the increase caused by the strain-dependent crystal-field splitting. Therefore the strain-induced changes of the hopping amplitudes appear to be crucial for the insulator-to-metal transition induced in $LaTiO_3$ under compressive strain. In contrast, in $LaVO_3$, the effects of crystal-field splitting and hopping amplitudes cooperate only for the case of tensile strain, whereas they essentially cancel each other under compressive strain. This is similar to the case of $SrVO_3$ discussed in Sec. IV A, and confirms the interpretation/discussion already given in Ref. [29].

V. SUMMARY AND CONCLUSIONS

In summary, we have studied the effect of epitaxial strain on the Mott MIT in various perovskite-structure TM oxides with d^1 and d^2 electron configuration of the TM cation, using first-principles-based DFT+DMFT calcuations. The MIT in

these materials is governed by the partially filled "t_{2g} bands", derived mainly from the corresponding orbitals of the TM cations. We have analyzed the effect of epitaxial strain on these bands in terms of strain-induced changes of the crystal-field splitting and hopping amplitudes.

Our results show that the strain-induced changes in the hopping amplitudes are qualitatively similar in all investigated systems. They favor the metallic state under compressive strain and the insulating state under tensile strain. In contrast, the strain-induced crystal-field splitting will generally always favor the insulating state, due to the reduced degeneracy of the lowest energy orbitals. Consequently, the effects of crystal-field and hopping amplitides usually cooperate under tensile strain, favoring the insulating state, while they can effectively cancel each other under compressive strain (see, e.g., the cases of $SrVO_3$ and $LaVO_3$).

Strong octahedral tilts can modify these general trends, as in the case of $LaTiO_3$. Here, the octahedral tilt distortion of the perovskite structure leads to a strong crystal-field splitting already in the unstrained state. This "built-in" crystal-field splitting resembles the splitting that is otherwise induced under tensile strain, and, as a result, compressive strain can induce a transition to the metallic state by increasing the effective orbital degeneracy. However, our calculations also demonstrate that the simultaneous strain-induced increase of the in-plane hoppings leads to a much stronger shift of the critical U compared to the crystal-field splitting alone.

Thus our results show that both the strain-induced changes in the crystal-field splitting and in the hopping amplitudes need to be considered to correctly describe the effect of epitaxial strain. Generally, the strain-induced changes in the hopping amplitudes can be equally important as the strain-induced changes in the crystal-field splitting for the overall behavior of the strained material.

A particularly strong effect can be expected under tensile strain, where the insulating state is strongly favored both by the strain-induced changes in the crystal-field and hopping parameters. This provides the possibility to move correlated metallic systems such as $SrVO_3$ or $CaVO_3$ closer to the insulating state, or even across the MIT, which is particularly interesting, e.g., for the recently proposed applications of these correlated metals as efficient transparent conductors [68].

The impact of epitaxial strain should also be accounted for in view of recent reports of MITs in ultrathin films of $SrVO_3$ [34] and $CaVO_3$ [35]. The insulating character observed in these ultrathin films has originally been attributed to a reduction in bandwidth due to the dimensional crossover from a three-dimensional metal to a two-dimensional insulator [34,35]. In contrast, Zhong *et al.* have recently argued that the crucial factor is instead the crystal-field splitting between the t_{2g} states that is caused by the reduced symmetry in such ultrathin films (which is of the same type as the one induced under tensile epitaxial strain) [66]. Here, we show that the strain-induced change in bandwidth is another important ingredient that can cooperate or—under compressive strain—compete with the crystal-field effect.

Finally, our work demonstrates that epitaxial strain indeed provides an effective route to tune the strength of electronic correlations and the vicinity to the Mott MIT in early TM perovskites. While further systematic investigations are required to study the interplay between strain and other effects occurring in thin films such as, e.g., interface effects, confinement, or defects, it is clear that strain is a very important factor determining the properties of thin films and heterostructures of correlated TM oxides.

ACKNOWLEDGMENTS

This work was supported by ETH Zurich and the Swiss National Science Foundation through Grant No. 200021_143265 and through the NCCR-MARVEL. Calculations have been performed on the PASC cluster "Mönch", hosted by the Swiss National Supercomputing Centre and the "Euler" cluster of the ETH Zurich.

[1] D. G. Schlom, L.-Q. Chen, X. Pan, A. Schmehl, and M. A. Zurbuchen, J. Am. Ceram. Soc. **91**, 2429 (2008).
[2] J. Li, Z. Shan, and E. Ma, MRS Bull. **39**, 108 (2014).
[3] D. G. Schlom, L.-Q. Chen, C. J. Fennie, V. Gopalan, D. A. Muller, X. Pan, R. Ramesh, and R. Uecker, MRS Bull. **39**, 118 (2014).
[4] N. A. Pertsev, A. G. Zembilgotov, and A. K. Tagantsev, Phys. Rev. Lett. **80**, 1988 (1998).
[5] K. J. Choi, M. Biegalski, Y. L. Li, A. Sharan, J. Schubert, R. Uecker, P. Reiche, Y. B. Chen, X. Q. Pan, V. Gopalan, L. Q. Chen, D. G. Schlom, and C. B. Eom, Science **306**, 1005 (2004).
[6] C. Ederer and N. A. Spaldin, Phys. Rev. Lett. **95**, 257601 (2005).
[7] J. H. Haeni, P. Irvin, W. Chang, R. Uecker, P. Reiche, Y. L. Li, S. Choudhury, W. Tian, M. E. Hawley, B. Craigo, A. K. Tagantsev, X. Q. Pan, S. K. Streiffer, L. Q. Chen, S. W. Kirchoefer, J. Levy, and D. G. Schlom, Nature (London) **430**, 758 (2004).
[8] J. H. Lee, L. Fang, E. Vlahos, X. Ke, Y. W. Jung, L. F. Kourkoutis, J.-W. Kim, P. J. Ryan, T. Heeg, M. Roeckerath, V. Goian, M. Bernhagen, R. Uecker, P. C. Hammel, K. M. Rabe, S. Kamba, J. Schubert, J. W. Freeland, D. A. Muller, C. J. Fennie, P. Schiffer, V. Gopalan, E. Johnston-Halperin, and D. G. Schlom, Nature (London) **466**, 954 (2010).
[9] Y. Suzuki, G. Hu, R. van Dover, and R. Cava, J. Magn. Magn. Mater. **191**, 1 (1999).
[10] J. A. Heuver, A. Scaramucci, Y. Blickenstorfer, S. Matzen, N. A. Spaldin, C. Ederer, and B. Noheda, Phys. Rev. B **92**, 214429 (2015).
[11] B. Yildiz, MRS Bull. **39**, 147 (2014).
[12] R. F. Berger, C. J. Fennie, and J. B. Neaton, Phys. Rev. Lett. **107**, 146804 (2011).
[13] W. S. Choi and H. N. Lee, Phys. Rev. B **91**, 174101 (2015).
[14] H. K. Yoo, S. I. Hyun, L. Moreschini, H.-D. Kim, Y. J. Chang, C. H. Sohn, D. W. Jeong, S. Sinn, Y. S. Kim, A. Bostwick, E. Rotenberg, J. H. Shim, and T. W. Noh, Sci. Rep. **5**, 8746 (2015).
[15] B. Burganov, C. Adamo, A. Mulder, M. Uchida, P. D. C. King, J. W. Harter, D. E. Shai, A. S. Gibbs, A. P. Mackenzie, R. Uecker,

M. Bruetzam, M. R. Beasley, C. J. Fennie, D. G. Schlom, and K. M. Shen, Phys. Rev. Lett. **116**, 197003 (2016).
[16] M. Imada, A. Fujimori, and Y. Tokura, Rev. Mod. Phys. **70**, 1039 (1998).
[17] J. Liu, M. Kareev, B. Gray, J. W. Kim, P. Ryan, B. Dabrowski, J. W. Freeland, and J. Chakhalian, Appl. Phys. Lett. **96**, 233110 (2010).
[18] S. Catalano, M. Gibert, V. Bisogni, O. E. Peil, F. He, R. Sutarto, M. Viret, P. Zubko, R. Scherwitzl, A. Georges *et al.*, APL Mater. **2**, 116110 (2014).
[19] J. H. Gruenewald, J. Nichols, J. Terzic, G. Cao, J. W. Brill, and S. S. Seo, J. Mater. Res. **29**, 2491 (2014).
[20] C. He, T. D. Sanders, M. T. Gray, F. J. Wong, V. V. Mehta, and Y. Suzuki, Phys. Rev. B **86**, 081401 (2012).
[21] K. Dymkowski and C. Ederer, Phys. Rev. B **89**, 161109 (2014).
[22] K. Yoshimatsu, H. Okabe, T. Oshima, S. Ueda, and A. Ohtomo, Phys. Rev. B **93**, 195159 (2016).
[23] H. Takagi and H. Y. Hwang, Science **327**, 1601 (2010).
[24] Z. Yang, C. Ko, and S. Ramanathan, Annu. Rev. Mater. Res. **41**, 337 (2011).
[25] A. Georges, G. Kotliar, W. Krauth, and M. J. Rozenberg, Rev. Mod. Phys. **68**, 13 (1996).
[26] K. Held, Adv. Phys. **56**, 829 (2007).
[27] A. Fujimori, I. Hase, H. Namatame, Y. Fujishima, Y. Tokura, H. Eisaki, S. Uchida, K. Takegahara, and F. M. F. de Groot, Phys. Rev. Lett. **69**, 1796 (1992).
[28] T. Arima, Y. Tokura, and J. B. Torrance, Phys. Rev. B **48**, 17006 (1993).
[29] G. Sclauzero and C. Ederer, Phys. Rev. B **92**, 235112 (2015).
[30] F. J. Wong, S.-H. Baek, R. V. Chopdekar, V. V. Mehta, H.-W. Jang, C.-B. Eom, and Y. Suzuki, Phys. Rev. B **81**, 161101 (2010).
[31] S. Okamoto and A. J. Millis, Nature (London) **428**, 630 (2004).
[32] N. Nakagawa, H. Y. Hwang, and D. A. Mueller, Nat. Mater. **5**, 204 (2006).
[33] P. R. Willmott, S. A. Pauli, R. Herger, C. M. Schlepütz, D. Martoccia, B. D. Patterson, B. Delley, R. Clarke, D. Kumah, C. Cionca *et al.*, Phys. Rev. Lett. **99**, 155502 (2007).
[34] K. Yoshimatsu, T. Okabe, H. Kumigashira, S. Okamoto, S. Aizaki, A. Fujimori, and M. Oshima, Phys. Rev. Lett. **104**, 147601 (2010).
[35] M. Gu, J. Laverock, B. Chen, K. E. Smith, S. A. Wolf, and J. Lu, J. Appl. Phys. **113**, 133704 (2013).
[36] G. Herranz, M. Basletić, M. Bibes, C. Carrétéro, E. Tafra, E. Jacquet, K. Bouzehouane, C. Deranlot, A. Hamzić, J. M. Broto, A. Barthélémy, and A. Fert, Phys. Rev. Lett. **98**, 216803 (2007).
[37] M. Basletic, J. L. Maurice, C. Carrétéro, G. Herranz, O. Copie, M. Bibes, É. Jacquet, K. Bouzehouane, S. Fusil, and A. Barthélémy, Nat. Mater. **7**, 621 (2008).
[38] U. Aschauer, R. Pfenninger, S. M. Selbach, T. Grande, and N. A. Spaldin, Phys. Rev. B **88**, 054111 (2013).
[39] E. Pavarini, S. Biermann, A. Poteryaev, A. I. Lichtenstein, A. Georges, and O. K. Andersen, Phys. Rev. Lett. **92**, 176403 (2004).
[40] H. T. Dang, X. Ai, A. J. Millis, and C. A. Marianetti, Phys. Rev. B **90**, 125114 (2014).
[41] N. Marzari, A. A. Mostofi, J. R. Yates, I. Souza, and D. Vanderbilt, Rev. Mod. Phys. **84**, 1419 (2012).
[42] F. Lechermann, A. Georges, A. Poteryaev, S. Biermann, M. Posternak, A. Yamasaki, and O. K. Andersen, Phys. Rev. B **74**, 125120 (2006).
[43] P. Werner, E. Gull, and A. J. Millis, Phys. Rev. B **79**, 115119 (2009).
[44] T. Kita, T. Ohashi, and N. Kawakami, Phys. Rev. B **84**, 195130 (2011).
[45] L. Huang, L. Du, and X. Dai, Phys. Rev. B **86**, 035150 (2012).
[46] A. I. Poteryaev, M. Ferrero, A. Georges, and O. Parcollet, Phys. Rev. B **78**, 045115 (2008).
[47] O. Gunnarsson, E. Koch, and R. M. Martin, Phys. Rev. B **54**, R11026 (1996).
[48] S. Florens, A. Georges, G. Kotliar, and O. Parcollet, Phys. Rev. B **66**, 205102 (2002).
[49] J. M. Rondinelli and N. A. Spaldin, Adv. Mater. **23**, 3363 (2011).
[50] V. I. Anisimov, I. A. Nekrasov, D. E. Kondakov, T. M. Rice, and M. Sigrist, Eur. Phys. J. B **25**, 191 (2002).
[51] A. Koga, N. Kawakami, T. M. Rice, and M. Sigrist, Phys. Rev. Lett. **92**, 216402 (2004).
[52] P. Hohenberg and W. Kohn, Phys. Rev. **136**, B864 (1964).
[53] W. Kohn and L. J. Sham, Phys. Rev. **140**, A1133 (1965).
[54] J. P. Perdew, K. Burke, and M. Ernzerhof, Phys. Rev. Lett. **77**, 3865 (1996).
[55] P. Giannozzi, S. Baroni, N. Bonini, M. Calandra, R. Car, C. Cavazzoni, D. Ceresoli, G. L. Chiarotti, M. Cococcioni, I. Dabo, A. D. Corso, S. de Gironcoli, S. Fabris, G. Fratesi, R. Gebauer, U. Gerstmann, C. Gougoussis, A. Kokalj, M. Lazzeri, L. Martin-Samos, N. Marzari, F. Mauri, R. Mazzarello, S. Paolini, A. Pasquarello, L. Paulatto, C. Sbraccia, S. Scandalo, G. Sclauzero, A. P. Seitsonen, A. Smogunov, P. Umari, and R. Wentzcovitch, J. Phys.: Condens. Matter **21**, 395502 (2009).
[56] D. Vanderbilt, Phys. Rev. B **41**, 7892 (1990).
[57] A. A. Mostofi, J. R. Yates, Y.-S. Lee, I. Souza, D. Vanderbilt, and N. Marzari, Comput. Phys. Commun. **178**, 685 (2008).
[58] K. Haule, T. Birol, and G. Kotliar, Phys. Rev. B **90**, 075136 (2014).
[59] E. Gull, A. J. Millis, A. I. Lichtenstein, A. N. Rubtsov, M. Troyer, and P. Werner, Rev. Mod. Phys. **83**, 349 (2011).
[60] O. Parcollet, M. Ferrero, T. Ayral, H. Hafermann, I. Krivenko, L. Messio, and P. Seth, Comput. Phys. Commun. **196**, 398 (2015).
[61] P. Seth, I. Krivenko, M. Ferrero, and O. Parcollet, Comput. Phys. Commun. **200**, 274 (2016).
[62] M. Aichhorn, L. Pourovskii, P. Seth, V. Vildosola, M. Zingl, O. E. Peil, X. Deng, J. Mravlje, G. J. Kraberger, C. Martins *et al.*, Comput. Phys. Commun. **204**, 200 (2016).
[63] M. Jarrell and J. E. Gubernatis, Phys. Rep. **269**, 133 (1996).
[64] M. Karolak, T. O. Wehling, F. Lechermann, and A. I. Lichtenstein, J. Phys.: Condens. Matter **23**, 085601 (2011).
[65] S. Fuchs, E. Gull, M. Troyer, M. Jarrell, and T. Pruschke, Phys. Rev. B **83**, 235113 (2011).
[66] Z. Zhong, M. Wallerberger, J. M. Tomczak, C. Taranto, N. Parragh, A. Toschi, G. Sangiovanni, and K. Held, Phys. Rev. Lett. **114**, 246401 (2015).
[67] M. De Raychaudhury, E. Pavarini, and O. K. Andersen, Phys. Rev. Lett. **99**, 126402 (2007).
[68] L. Zhang, Y. Zhou, L. Guo, W. Zhao, A. Barnes, H.-T. Zhang, C. Eaton, Y. Zheng, M. Brahlek, H. F. Haneef, N. J. Podraza, M. H. W. Chan, V. Gopalan, K. M. Rabe, and R. Engel-Herbert, Nat. Mater. **15**, 204 (2015).
[69] S. Biermann, J. Phys.: Condens. Matter **26**, 173202 (2014).
[70] P. Werner and M. Casula, J. Phys.: Condens. Matter **28**, 383001 (2016).